Journal of Power Sources 225 (2013) 51–59

Contents lists available at SciVerse ScienceDirect

Journal of Power Sources

journal homepage: www.elsevier.com/locate/jpowsour

Electrochemical behavior of solid oxide fuel cell anodes based on infiltration of Y-doped $SrTiO_3$

Alireza Torabi*, Thomas H. Etsell

Department of Chemical & Materials Engineering, University of Alberta, Edmonton, Alberta T6G 2G6, Canada

HIGHLIGHTS

- Y-doped $SrTiO_3$ infiltrated porous YSZ was investigated as an alternative anode.
- Amount of infiltrate must be optimized to balance conductivity and polarization.
- Heat treatment conditions highly affect the purity and crystal size.
- Electrochemical performance of the infiltrated anodes is highly enhanced.
- H_2S remarkably boosts the electrochemical performance under methane fuel.

ARTICLE INFO

Article history:
Received 2 August 2012
Received in revised form
25 September 2012
Accepted 27 September 2012
Available online 17 October 2012

Keywords:
Solid oxide fuel cells
Anode
Y-doped $SrTiO_3$
Infiltration
H_2S

ABSTRACT

Single cells based on yttrium-doped $SrTiO_3$ (YST) infiltrated porous YSZ anodes were investigated as an alternative material for sulfur and carbon tolerant solid oxide fuel cells. First, a YSZ electrolyte-based cell with porous YSZ as the support for electrode materials on both sides was prepared. Then electrocatalyst materials were incorporated into the porous YSZ: the anode was infiltrated with YST precursor; and the cathode with LSM precursor to be heat treated in-situ. Heat treatment under reducing conditions was found to successfully eliminate the yttrium titanate impurity and to markedly reduce the YST crystal size. The results showed that there was an optimum amount of infiltrated YST to balance the conductivity and the polarization. Furthermore, the maximum power density under dry hydrogen at 900 °C was found to be 95 mW cm^{-2}, which is greater than comparable reported values. H_2S was found to have a promoting effect on the electrochemical performance of the fuel cell, particularly under methane. This work suggests that the infiltration technique can be successfully used not only to eliminate the complications associated with high temperature treatments required in conventional YST-YSZ anodes, but also to improve the electrochemical performance.

1. Introduction

State-of-the-art SOFCs are undoubtedly those based on Ni-YSZ composite anodes. They demonstrate long term stability, low polarization, high electrical and thermal conductivity, and excellent catalytic activity [1–3]. In this cerment, Ni acts as an electronic conductor as well as a catalyst for the hydrogen oxidation reaction and YSZ provides a structural support to suppress the sintering of Ni, introduces mixed ionic–electronic conduction (MIEC), and more closely matches the thermal expansion of the anode to that of the other cell components. There are, however, several important drawbacks to Ni-YSZ anodes.

Performance degradation caused by microstructural change due to Ni phase coarsening is a critical concern in long term operation of the Ni-YSZ based SOFCs. Poor wettability of YSZ by nickel metal is known as the main cause of this agglomaration [4,5]. The sintering of Ni particles will result in the formation of isolated islands thus degrading the anode conductivity. While optimization of the cermet microstructure can address this problem to a great extent, cell operation at high current densities and fuel utilization can still lead to Ni phase coarsening [2].

In addition, poor mechanical stability during reduction/oxidation cycles is another significant challenge of Ni-based anodes. Although the anode normally performs under reducing conditions, several reduction/oxidation (redox) cycles might accidentally occur during its lifetime because of failure in the fuel supply, a broken seal, substantial fuel utilization, maintenance and so on [6]. When a cell experiences a redox cycle, the anode goes through

* Corresponding author. Tel.: +1 416 8875100.
E-mail addresses: torabite@ualberta.ca, atorabit@gmail.com (A. Torabi).

0378-7753/$ – see front matter © 2012 Elsevier B.V. All rights reserved.
http://dx.doi.org/10.1016/j.jpowsour.2012.09.109

a considerable volume change which causes a great deal of mechanical stress on the Ni-YSZ electrode. This severely threatens the cell integrity especially in an anode supported cell and may result in catastrophic failure.

Finally, in spite of the fact that one of the greatest advantages of SOFCs over other fuel cells is fuel flexibility, Ni-YSZ anodes are only compatible with hydrogen fuel. When more commercial fuels such as natural gas and synthesis gas are considered [3,7], impurities in these practical fuels even as low as a few ppm could severely degrade cell performance and affect its durability. Such loss is mainly due to the great sensitivity of Ni to various impurities including H_2S which is the most prevalent impurity that is unavoidably present in fuels like natural gas and synthesis gas [7]. Ni-based anodes are poisoned by H_2S levels as low as 0.05 ppm. It has been revealed that sulfur poisoning of Ni-based anodes involves two different stages [8]. At lower concentrations of H_2S (below 5 ppm), the interfacial adsorption of sulfur-based species on nickel, which is associated with a small voltage drop, is reversible. On the other hand, at higher concentrations of H_2S, sulfur poisoning of the anode leads to a large fatal voltage drop which is no longer reversible. In addition to being highly sensitive to fuel impurities, nickel is also not compatible with hydrocarbon fuels because of the carbon deposition problem [9,10]. The undesirable complications associated with the build up of carbon on Ni includes blocking of active sites on the anode, loss of nickel catalyst, and loss of structural integrity [11].

Recently, numerous studies have been undertaken with respect to alternative anode materials. These novel anodes have been developed based on two different approaches: ceramic–metal composites and oxide ceramics. The former is based upon a partial or total replacement of Ni with more impurity tolerant metals which have less propensity for carbon formation and/or substitution of the YSZ component by new electrolyte materials with greater ionic conductivity and higher stability [12]. The latter, on the other hand, utilizes oxides with both ionic and electronic conductivity at high temperatures under reducing conditions. Higher compatibility with the electrolyte, improved long term stability, and greater impurity tolerance and resistance to carbon deposition are the major advantages of oxide anodes over cermets [12,13].

Among the potential oxides, Y-doped $SrTiO_3$ (YST) is one of the most intriguing materials because of high electrical conductivity in a typical reducing atmosphere at an anode and close thermal expansion compatibility with YSZ [14]. Hui and Petric's work [15] is perhaps the landmark that demonstrated high electrical conductivity and chemical stability of this oxide anode. They pointed out that the level of reduction, which controls the conductivity, strongly depended on the partial pressure of oxygen in the reducing atmosphere and the saturation level of yttrium dopant. Ma et al. [16] showed that preparation and processing procedures for YST-based anodes including chemical composition, sintering temperature and sintering atmosphere critically affect cell performance. They concluded that, with respect to electrical conductivity and redox stability, 2–6% A-site deficient YST is very promising. Fu et al. [17] reported that the conductivity of YST is primarily governed by the concentration of Ti^{3+}; therefore, when YST is sintered at high temperatures under reducing conditions, the conductivity is highly improved. They argued that a high temperature post-reduction treatment is essential to develop a highly conductive YST. However, Ma et al. [18] revealed that such high temperature treatment leads to Ti diffusion from YST to YSZ. Not only could this diffusion introduce electronic conductivity into the YSZ electrolyte, but it also noticeably decreases the conductivity of YST.

In this study, in order to avoid complications posed by a high temperature treatment, a low temperature in-situ procedure was developed with a solution impregnation technique to prepare YST-based anodes. A well connected nano-sized YST network on a porous YSZ support was established and the electrochemical performance of such an anode under hydrogen and methane without and with H_2S impurity was characterized in detail.

2. Experimental procedure

2.1. Cell fabrication

YSZ discs (FuelCellMaterials, Lewis Center, OH, diameter: 25 mm, average thickness: 0.3 mm) were used as the electrolyte as well as the mechanical support. Thin porous YSZ scaffolds were used as supports for the anode and cathode electrocatalysts. The fabrication procedure for the thin porous YSZ layers has been explained in detail elsewhere [19]. First, as received YSZ (Tosoh TZ-8Y, Grove City, OH) was calcined at 1500 °C for 3 h and ball milled for 72 h. This calcined-milled YSZ (CYSZ) was used as the starting material for the thin porous scaffolds. Then, the CYSZ powder was well mixed with polymethyl methacrylate ((PMMA), Microbeads®, Spheromers CA 6, Norway) as a pore former (80 vol.% CYSZ + 20 vol.% PMMA). A laboratory-made ink (α-terpineol + 5 wt % ethylcellulose) was added to the mixed powder and they were well mixed in a mortar and pestle to leave a homogenous paste. Finally, YSZ coatings (diameter: 10 mm, average thickness: 25 μm) were screen printed onto the YSZ discs (both sides) followed by drying at 150 °C for 15 min and sintering at 1300 °C for 3 h. The characteristics of this porous support were indicated elsewhere in detail [19].

To prepare a stable solution for $Sr_{0.88}Y_{0.08}TiO_3$, $Y(NO_3)_3 \cdot 6H_2O$ (Alfa Aesar, 99.9% (REO)), $Sr(NO_3)_2$ (Alfa Aesar, ACS, 99.0% min), and $Ti[OCH(CH_3)_2]_4$ (Alfa Aesar, VERTEC® TIPT, 97+%) were used as the starting precursors. First, a solution of 1 mol titanium isopropoxide in 4 mol triethanolamine (Alfa Aesar, 98+%) and aqueous solutions of yttrium nitrate (3 mol L^{-1}) and strontium nitrate (3 mol L^{-1}) were prepared. Then, the correct molar ratios of the nitrates were mixed into the stabilized titanium isopropoxide solution to leave a stable solution named Sol-T. In order to prepare YST powders for phase analysist, 10 mL of this solution was dried at 150 °C/1 h and heat treated at 350 °C/1 h that resulted in a black porous mass. It was then heat treated for 6 h under air in a temperature range of 750–1400 °C.

In the current work, in order to understand whether the synthesis process would affect the final phase/phases or not, $Sr_{0.88}Y_{0.08}TiO_3$ was also synthesized by Pechini's method [20]. Similar to the above-mentioned method, $Ti[OCH(CH_3)_2]_4$ was used as the starting precursor. The molar ratio of Ti cation, complexing agent (citric acid, CA) and ethylene glycol in the solution was 1:2:10. First, titanium isopropoxide was added to ethylene glycol and mixed thoroughly in a beaker. While the solution was being mixed by a magnetic stirrer at ambient temperature, citric acid was gently introduced. An overnight stirring was enough to leave a clear and stable solution. 3 mol L^{-1} aqueous solutions of yttrium nitrate + CA and strontium nitrate + CA were prepared in which the metal cation to CA ratio was 1:2. The correct molar ratios of the nitrate solutions were then mixed into the stabilized titanium isopropoxide solution to leave another stable solution named Sol-P. The final heat treatment procedure of Sol-P was exactly the same as that of Sol-T.

Finally, to study the evolution of YST crystals from Sol-T and Sol-P, a Setaram Labsys Evo Differential Scanning Calorimeter (DSC) was utilized. The solutions (Sol-T and Sol-P) were dried at 150 °C/1 h. 50 mg of the dried/ground powder was then put in an alumina crucible and the sample was heated from room temperature up to 1200 °C at 5 °C min^{-1}. The alumina crucible was tested as

a blank with the same heating regime and the corresponding heat was subtracted from the powder heat profile. Also, an 800 °C isothermal DSC experiment was carried out. YST-T dried precursor was heat treated at 600 °C/1 h to ensure that all the combustion reactions occurred and the organic constituents were removed. This was used as the starting powder for the isothermal test. 50 mg of a heat treated/ground powder was put in an alumina crucible and the sample was heated from room temperature to 800 °C at 200 °C min^{-1} and kept at 800 °C for a period of 12 h.

To prepare the $Sr_{0.88}Y_{0.08}TiO_3$ infiltrated porous YSZ electrode, the thin porous electrode supports were infiltrated with the solution followed by a two step heat treatment process: 150 °C/5 min and 350 °C/15 min. This procedure was repeated until the desirable amount of YST was embedded into the YSZ network. The final heat treatment was done under either hydrogen or air at different temperatures which will be discussed later. A heat treated coating was examined by X-ray diffraction (XRD, Rigaku Ultima IV, Co Kα radiation) which confirmed the presence of YST nano-crystals along with YSZ.

Two types of cells were prepared in the current work: symmetrical cells to study the electrochemical behavior of YST infiltrated YSZ electrodes under open circuit voltage condition, and fuel cells to study the performance under potentiodynamic and potentiostatic conditions. To prepare the former, the above-mentioned procedure was symmetrically followed on both electrodes. For the fuel cell, however, this process was carried out only for the anode. For the cathode, $La_{0.8}Sr_{0.2}MnO_3$ (LSM) was chosen to be infiltrated into the porous YSZ support. $Mn(NO_3)_2 \cdot xH_2O$, $La(NO_3)_3 \cdot 6H_2O$ and $Sr(NO_3)_2$ (Alfa Aesar) were used as the starting precursors to prepare a solution based on Pechini's technique [21]. The molar ratio of metal cations, complexing agent (citric acid) and ethylene glycol in the solution was 1:4:4. The thin porous support was repeatedly impregnated by incipient wetness (10 times, on average) on the cathode side until 20 vol.% LSM was embedded into the YSZ network with the LSM phase to be formed in-situ. Post-XRD analysis on the cathode side confirmed the presence of an LSM nano-crystal phase along with YSZ.

2.2. Cell test

A laboratory made gold paste was used as a current collector (atomized gold powder, Technic Inc., Cranston, Rhode Island) on both electrodes. For the symmetrical cell test, the electrochemical behavior of the cells under open circuit condition was studied by ac impedance spectroscopy (Solartron 1255 frequency response analyzer in combination with a Solartron 1287 electrochemical interface) with a four probe configuration. The cells were heated up to 900 °C under humidified hydrogen with a constant flow rate of 50 mL min^{-1} (a room temperature bubbler was used to humidify the fuels), held for an hour and cooled down to 800 °C. Impedance measurements were carried out under open circuit condition over a frequency range from 0.1 Hz to 100 kHz with a 10 mV ac perturbation at 800, 850 and 900 °C.

For the fuel cell test, the anode side of the cell were sealed onto an alumina tube using a glass seal (Aremco 617). The anode electrode was exposed to humidified hydrogen with or without H_2S (ppm level) with a constant flow rate of 50 mL min^{-1}. Also, extra dry air (H_2O < 10 ppm) flowed through the cathode electrode at a similar rate. Ac impedance spectroscopy as well as potentiodynamic and potentiostatic analysis were carried out on the fuel cells with a four probe configuration to study the electrochemical behavior at 800, 850 and 900 °C.

2.3. Cell characterization

To compare the phases present before and after cell tests, post-XRD analysis was performed. Also the microstructure of the electrodes both before and after electrochemical testing was examined on fractured surfaces with a JEOL 6301F field emission scanning electron microscope (FE-SEM).

3. Results and discussion

3.1. Phase analysis

It is well acknowledged that Y-doped $SrTiO_3$ with vacancies on the Sr site (2–6%) shows higher electronic conductivity comparing to stoichiometric or Ti-site deficient compositions [16]. This is why $Sr_{0.88}Y_{0.08}TiO_3$ was chosen as the nominal starting composition. Obtaining the pure desirable phase was, however, quite challenging. Fig. 1 illustrates the XRD spectra of the YST powders obtained from heat treatment of Sol-T at 775, 800, 900 and 1400 °C under air for a period of 6 h. As observed, well defined peaks at 775 °C indicate that the YST crystallites are well developed. No extra phase was present at this temperature at least within the detection limit of the instrument. At 800 °C, however, yttrium titanate ($Y_2Ti_2O_7$) appeared as a minor phase. Increasing the temperature not only sharpened the peaks as expected indicating that the crystal size increased, but it also increased the fraction of this pyrochlore phase.

Ma et al. [16] and Lu et al. [22] have also reported the presence of $Y_2Ti_2O_7$ for a variety of compositions. Lu et al. used a modified Pechini process to synthesize an A-site deficient Y-doped $SrTiO_3$ with a nominal composition of $Sr_{0.86}Y_{0.08}TiO_3$ and reported the presence of $Y_2Ti_2O_7$ and TiO_2 (rutile) as minor impurities. No footprint of the rutile phase, however, was detected in this study. For the sake of comparison and to understand whether the synthesis process would affect the final phase/phases or not, $Sr_{0.88}Y_{0.08}TiO_3$ was also synthesized by Pechini's method (Sol-P). Again, 800 °C was the critical temperature below which no secondary phase was present and above which the pyrochlore phase appeared. It is noteworthy that the size and broadness of peaks were rather similar for YST obtained from Sol-T and Sol-P.

As discussed above, 800 °C is a critical temperature for the appearance of $Y_2Ti_2O_7$. In order to see if this can also be confirmed by thermal analysis, a series of DSC tests was carried out on both Sol-T and Sol-P precursors. Fig. 2(a) shows how the heat changes with temperature. As observed, the exothermic combustion reactions are all completed before 500 °C in both cases. Interestingly, there is a slight slope change in both curves at about 800 °C. Obviously, the slope change is not significant which is not unexpected because the amount of the pyrochlore phase is very minor. To confirm such a heat change at the critical temperature, an isothermal test was done at 800 °C and the result appears in Fig. 2(b). Once the temperature reached 800 °C, the heat stayed

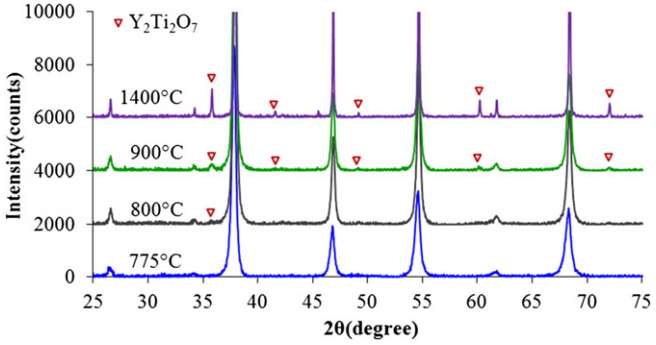

Fig. 1. XRD spectra of the YST powders obtained from heat treatment of Sol-T at 775, 800, 900 and 1400 °C under air for a period of 6 h.

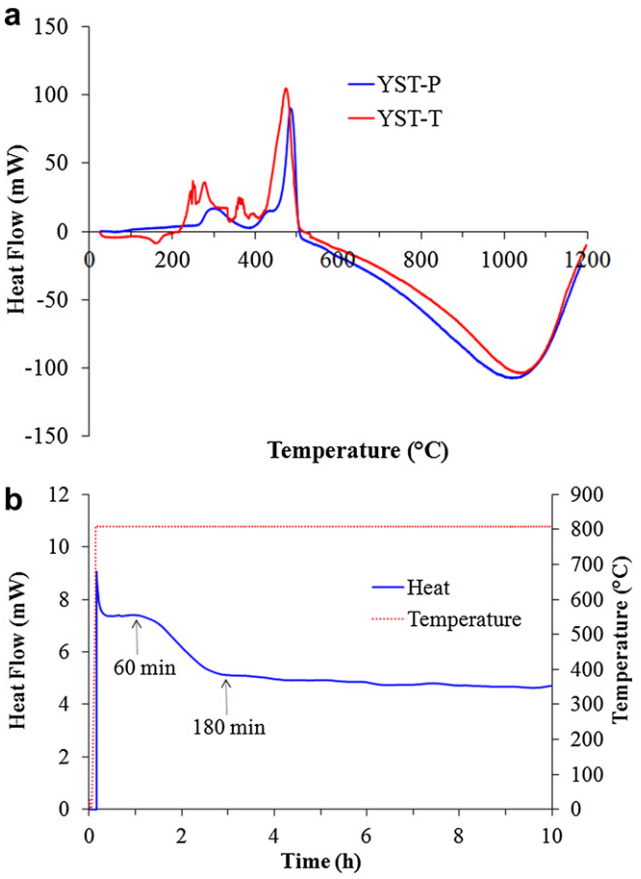

Fig. 2. (a) DSC spectrum of Sol-T and Sol-P, (b) Isothermal DSC spectrum of Sol-T at 800 °C.

reasonably unchanged during the first hour. A decrease in heat flow was observed in the next 2 h and from then it remained virtually constant. Thus, in agreement with XRD analysis, thermal analysis also suggests that the very minor yttrium titanate impurity is unavoidably formed at about 800 °C.

The effect of synthesis atmosphere was also studied. First single phase YST powders were synthesized from Sol-T and Sol-P at 750 °C/6 h under air. The YST obtained then experienced a final treatment at 900 °C/6 h and 1200 °C/6 h under different atmospheres including air, oxygen, 10% hydrogen balance argon, and hydrogen. No matter what the solution precursor, post treatment atmosphere and temperature were, the synthesized YST powders contained a very minor amount of $Y_2Ti_2O_7$. It was, thus, concluded that the presence of this minor phase is almost unavoidable. In one case, the synthesis procedure was carried out under reducing conditions from the very beginning. YST-T solution was dried at 150 °C/1 h and then heat treated under hydrogen from room temperature up to 900 °C for 6 h. The XRD spectra of YST powder synthesized under air and hydrogen at 900 °C/6 h are compared in Fig. 3. Surprisingly, the powder synthesized under reducing conditions was pure YST with no $Y_2Ti_2O_7$ secondary phase. More importantly, the characteristic YST peaks are noticeably broader meaning that the crystallites were finer.

3.2. Symmetrical studies

The ac impedance spectra of three different YST-YSZ symmetrical cells at 800 °C under humidified hydrogen fuel are shown in Fig. 4(a). It is important to note that the impedance data in this

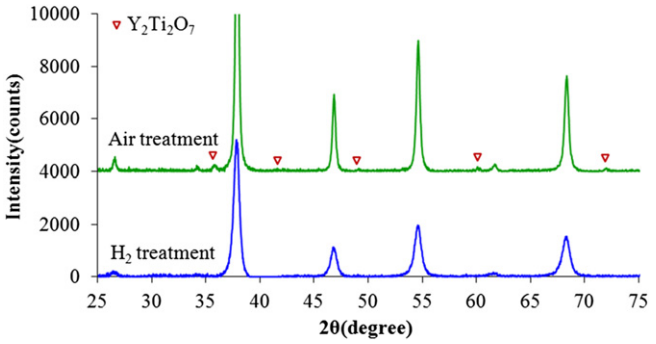

Fig. 3. XRD spectra of YST powder synthesized under air and hydrogen at 900 °C/6 h.

figure represent half cell polarizations. This means that all the data from a symmetrical cell with two YST-YSZ electrodes and a 300 μm electrolyte were halved and, therefore, the polarization of only one YST-YSZ electrode and a 150 μm electrolyte is shown. This is indeed the case for all the symmetrical data presented in this study. While these samples were equally infiltrated four times with a two step low temperature air treatment (150 °C/5 min and 350 °C/15 min) after each infiltration step using the Sol-T, they were subjected to different high-temperature heat treatment procedures: YST-A was infiltrated four times and finally heat treated at 900 °C/6 h under air. YST-H was infiltrated four times and finally heat treated at 900 °C/6 h under hydrogen. As for the YST-A-H cell, it was first infiltrated twice followed by a treatment at 900 °C/6 h under air. Then, it was infiltrated two more times followed by a final treatment at 900 °C/6 h under hydrogen. The final YST gain was 23 wt% for the three samples.

Interestingly, while the ohmic resistances of these cells are virtually identical, their non-ohmic polarizations are quite varied. The polarization spectra comprise two semicircles: One arc in the high-medium frequency range (100 kHz–100 Hz) and one in the low frequency range (<100 Hz). The former is normally attributed to charge transfer resistance corresponding to electron–ion transfer processes occurring at the interfaces [23,24], and the latter is predominantly attributed to non-charge transfer processes including surface reactions as well as solid state and gas phase diffusion [23,25]. As observed in Fig. 4(a), while the high-medium frequency range semicircles are rather similar for these cells, the

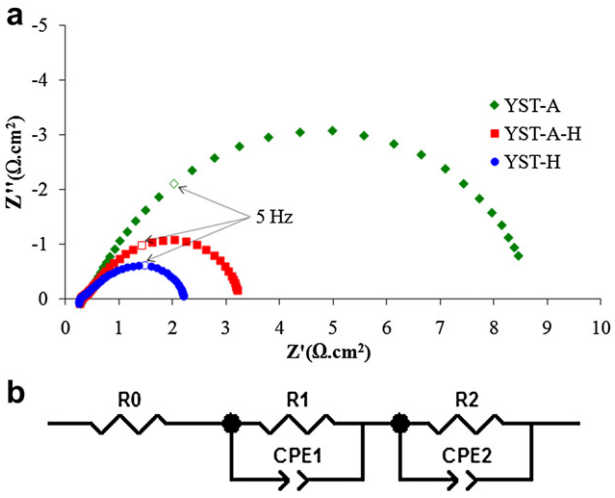

Fig. 4. (a) Ac impedance spectra of three different YST–YSZ symmetrical cells at 800 °C under humidified hydrogen fuel, (b) an equivalent circuit model.

low frequency range arcs are very different indicating that the non-charge transfer polarization is significantly affected by the heat treatment procedure. An equivalent circuit is also shown in Fig. 4(b) which includes the ohmic resistance corresponding to the YSZ electrolyte (R_0), and the non-ohmic polarization corresponding to the composite electrode (R_1 and R_2). For the sake of comparison, the ohmic and non-ohmic polarizations of the cells are summarized in Table 1.

This comparison helps to understand what gives rise to the non-charge transfer polarization difference. As described above, except for the high temperature treatment atmosphere during YST synthesis, these cells are essentially identical. It was already shown in Fig. 3 that when the YST heat treatment is performed under hydrogen, the final YST crystallites are clearly smaller. The calculated crystal size of YST using XRD line broadening and the Scherrer equation was about 36 and 16 nm for air and hydrogen treated samples, respectively. Thus, this implies that the low frequency arc is the corollary of surface reactions. Since the hydrogen treated cell has finer YST crystallites comparing to the air treated one, it is reasonable that its surface reaction polarization is smaller (1.99 Ω cm^2 as opposed to 8.30 Ω cm^2). The fact that the surface reaction polarization of the YST-A-H cell is between the other two (2.77 Ω cm^2) sensibly supports this argument.

Fig. 5 shows how the amount of YST incorporated into the porous YSZ support affects both conductivity and total polarization (the difference between the high frequency and low frequency intercepts with the real axis) of the symmetrical cells. The impedance spectra of three cells are compared in this figure at 800 and 900 °C under humidified hydrogen atmosphere in which the number of infiltration cycles are 1, 4 and 8, and the final wt% of YST (based on the porous support weight) are 13, 23 and 35.5, respectively. A similar equivalent circuit model was used (Fig. 4(b)) to deconvolute the polarization which includes the ohmic resistance (R_0) and the non-ohmic polarizations (R_1 and R_2) of the cells. For the sake of comparison, the ohmic resistance, non-ohmic polarizations, and the total polarization of these cells based on the fit data are summarized in Table 2.

As expected, the more YST incorporated into the composite, the less the ohmic resistance of the cell. For example, the ohmic resistances at 800 °C are 0.38, 0.34 and 0.30 Ω cm^2 for cells with 13, 23 and 35.5 wt% YST, respectively. This is, indeed, not the case for the non-ohmic polarization. Interestingly, while the change in charge transfer polarization (high-medium frequency arc, R_1) is quite minor, the non-charge transfer polarization (low frequency semicircle, R_2) experiences a significant change. When the amount of incorporated YST increases, three phase boundaries (TPBs), where the ion-conducting phase (YSZ), the electron conducting phase (YST) and the gas phase (hydrogen) coexist, increase. However, if the infiltration is overdone, the YSZ porous support is fully covered with a uniform YST coating and the electrochemical reaction sites are limited to those at the electrode–electrolyte interface and, therefore, the TPBs decrease. Since the change in TPBs reveals itself as the change in R_2 in the impedance spectra, this confirms the above mentioned argument that the low frequency polarization is attributed to surface reaction polarization. This suggests that there is an optimum amount of infiltrated YST to balance the conductivity and the polarization. The optimum essentially depends on the specific surface area of the support and the particle size of the infiltrated component [19].

Table 1
Ohmic and non-ohmic polarization of YST infiltrated YSZ symmetrical cells with different treatments.

Cell	R_0 (Ω cm^2)	R_1 (Ω cm^2)	R_2 (Ω cm^2)
YST-A	0.30	0.28	8.30
YST-A-H	0.29	0.26	2.77
YST-H	0.29	0.20	1.99

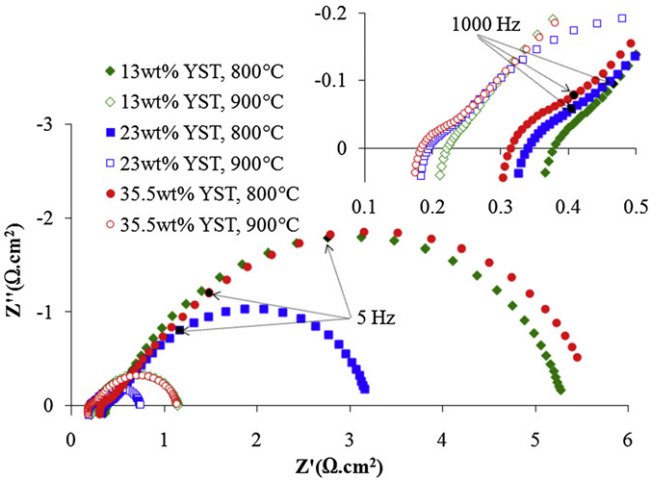

Fig. 5. Ac impedance spectra of YST infiltrated YSZ symmetrical cells with 13, 23 and 35.5 wt% YST.

The anode/electrolyte interface of these three cells is illustrated in Fig. 6. Comparison between the micrographs reasonably supports the above mentioned argument on TPBs. 13 wt% YST (Fig. 6(a)) is obviously not enough to fully cover the porous support. Such poor coverage results in not only higher ohmic resistance, but also greater reaction polarization. When the amount of YST is 23% (Fig. 6(b)), however, the porous support is reasonably covered with well connected nano-sized YST particles, causing a reasonable balance between conductivity and polarization. Finally, in the cell with 35.5 wt% YST (Fig. 6(c)), the whole support is covered with a relatively thick YST film, which undoubtedly favors conductivity but not polarization.

The effect of fuel composition on the electrochemical behavior of the YST infiltrated cells is illustrated in Fig. 7. The ac impedance spectra of a 23 wt% YST infiltrated YSZ symmetrical cell at 800 °C under four different humidified fuels including hydrogen, hydrogen + 100 ppm H_2S, hydrogen + 1000 ppm H_2S, and methane are presented. The ohmic resistance (R_0) and the charge transfer polarization (R_1) do not depend on the atmosphere, whereas the non-charge transfer polarization is noticeably affected by the fuel composition. As discussed above, the low frequency polarization (R_2) is attributed to surface reactions. It is not surprising, thus, that when hydrogen is compared with methane, such polarization is a lot higher simply because methane is much harder to activate at 800 °C [26]. Unexpectedly, the surface reaction polarization turned out to be improved by adding ppm levels of H_2S to the humidified hydrogen. The surface reaction polarizations are 2.97, 2.80 and 2.43 Ω cm^2 for humidified hydrogen fuel with 0, 100 and 1000 ppm of H_2S, respectively. A 6 and 18% decrease in the surface polarization is observed upon the addition of 100 and 1000 ppm of H_2S (such performance improvement will be discussed later).

Table 2
Ohmic and non-ohmic polarization of YST infiltrated YSZ symmetrical cells with different YST content.

YST content (wt%)	R_0 (Ω cm^2)		R_1 (Ω cm^2)		R_2 (Ω cm^2)	
	800 °C	900 °C	800 °C	900 °C	800 °C	900 °C
13	0.38	0.22	0.29	0.14	4.93	0.79
23	0.34	0.19	0.32	0.14	2.61	0.41
35.5	0.30	0.18	0.33	0.15	5.24	0.82

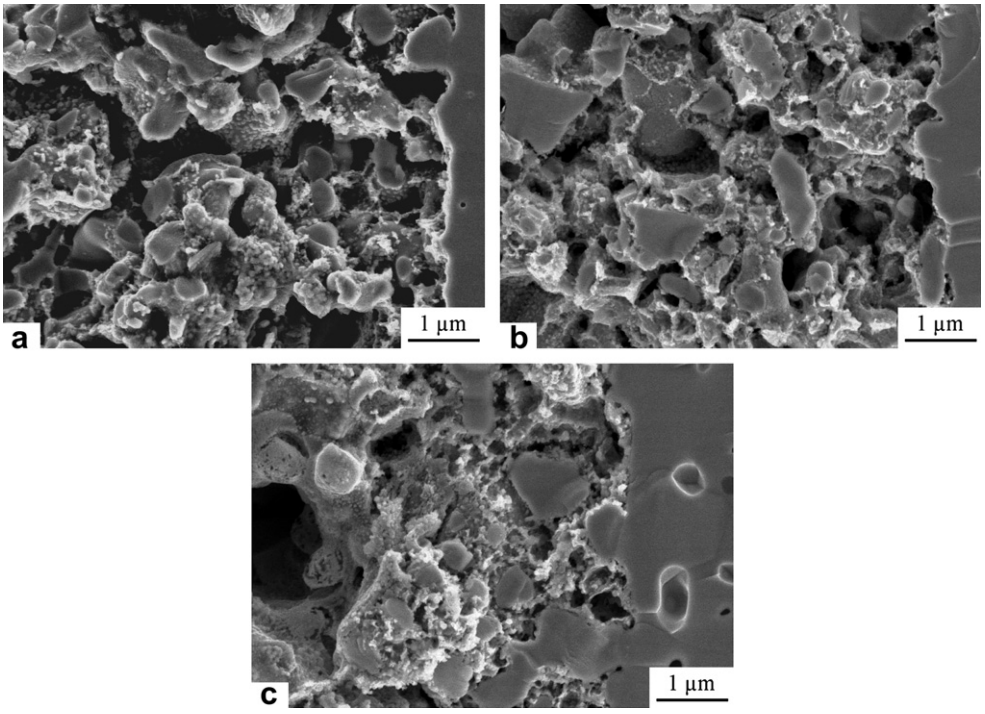

Fig. 6. SEM micrographs of the anode/electrolyte interface of YST infiltrated YSZ symmetrical cells with (a) 13, (b) 23 and (c) 35.5 wt% YST.

3.3. Fuel cell studies

The electrochemical performance of a cell with a 23 wt% YST infiltrated YSZ anode is shown in Fig. 8 including (a) open circuit impedance spectra and (b) *V*–*i* characteristics and power densities at 850 °C under humidified hydrogen fuel with different contents of H_2S. Similar to the above described symmetrical studies on YST infiltrated anodes, we have previously studied the electrochemical behavior of symmetrical LSM infiltrated YSZ cathodes [19]. Considering the fact that the polarization resistance of the LSM infiltrated YSZ cathode under OCP is very low (about 0.15 Ω cm^2 at 800 °C), the rather large polarization resistance of a YST infiltrated YSZ anode/YSZ electrolyte/LSM infiltrated YSZ cathode cell can be reasonably attributed to the anode electrode. The fact that the characteristics of the impedance spectra of the fuel cell (Fig. 8(a)) strongly resemble that of the symmetrical one (Fig. 7(a)) supports this argument.

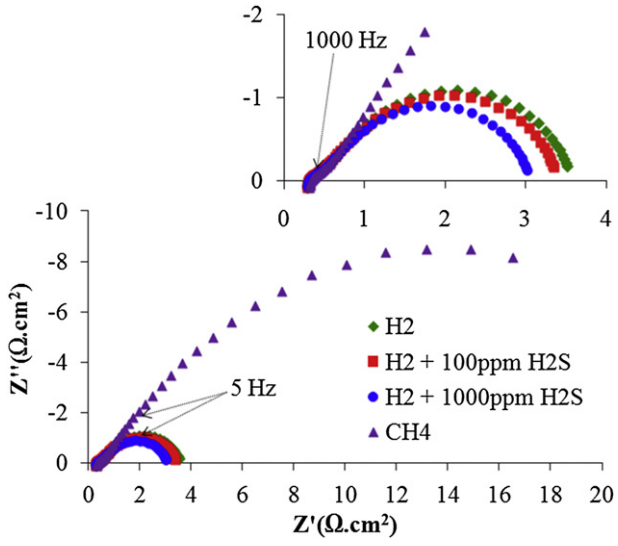

Fig. 7. Ac impedance spectra of YST infiltrated YSZ symmetrical cell under various fuels.

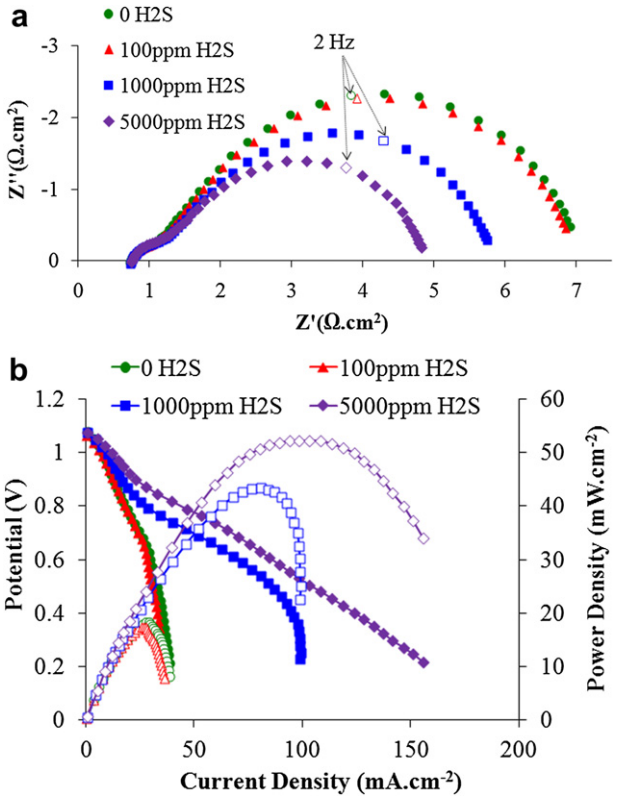

Fig. 8. Electrochemical performance of the cell with 23 wt% YST infiltrated YSZ anode: (a) open circuit impedance spectra and (b) *V*–*i* characteristics and power densities at 850 °C under humidified hydrogen fuel with different H_2S content.

The effect of H_2S on the cell performance is quite unexpected; not only does the performance not deteriorate, but it is greatly improved with H_2S. Similar to symmetrical cell behavior under H_2S, the performance improvement reveals itself as a decrease in low frequency polarization (R_2) in the impedance spectra. While the ohmic resistance (R_0) and the charge transfer polarization (R_1) are unaffected, the surface reaction polarization is remarkably improved with H_2S. For the sake of comparison, R_2 is 5.78, 5.68, 4.21 and 3.28 Ω cm^2 for humidified hydrogen fuel with 0, 100, 1000 and 5000 ppm of H_2S, respectively, based on the fit data. This suggests that H_2S plays a catalytic role and promotes the fuel oxidation reaction.

The V–i characteristics and power densities in Fig. 8(b) also show the promotion effect of H_2S. While the maximum power densities under humidified hydrogen with no H_2S and 100 ppm H_2S are relatively poor (about 18 mW cm^{-2}), addition of 0.1 and 0.5% H_2S increases the power densities by a factor of 2.4 and 2.9, respectively. It is known that at low current densities, activation polarization contributes the most to the cell voltage losses, indicated by the rather sharp drop in cell voltage with increasing current. As shown in this figure, the more H_2S introduced into the hydrogen fuel, the less the activation polarization is. When the current density increases further, ohmic resistance dominates and the voltage decreases linearly. In Fig. 8(b), such a linear region is only distinct when the fuel contained 0.1 and 0.5% H_2S. Eventually, at higher current densities, the cell polarization is governed by mass transfer limitations and a relatively sharp voltage loss is expected. It is interesting that when the cell was operated on zero or lower H_2S content fuels, mass transfer polarization was rather severe. However, no mass transfer limitation was observed when the H_2S level was as high as 5000 ppm. Phase analysis after the performance measurement (not shown here) confirmed that YSZ and YST were chemically stable and no sulfur poisoning was detected in the doped strontium titanate phase at H_2S levels as high as 5000 ppm.

Shown in Fig. 9, the electrochemical performance of this cell was also studied under humidified methane without H_2S and with 5000 ppm H_2S. The open circuit impedance spectra are illustrated in Fig. 9(a) and V–i characteristics and power densities at 850 °C under humidified methane fuel with different contents of H_2S are presented in Fig. 9(b). Very interestingly, the effect of H_2S on electrochemical performance improvement is quite dramatic. Under humidified methane, the cell performance is absolutely poor. The total cell polarization is more than 160 Ω cm^2 and the maximum power density is about 1.1 mW cm^{-2}. However, when the fuel contained 0.5% H_2S, the total polarization dropped to 4.7 Ω cm^2 and the maximum power density jumped to slightly more than 37 mW cm^{-2}. This indicates than the electrochemical performance improves by a factor of about 35 when the methane fuel contains 5000 ppm H_2S.

The promoting effect of H_2S on electrochemical performance of ceramic fuel cells with lanthanum doped strontium titanate (LST) has been previously reported [27,28]. Vincent et al. [28] showed that not only does H_2S play a role as a fuel, but more importantly it improves the electrochemical oxidation of the primary fuel, i.e., methane. For example, while the maximum power density of a cell based on an LST-YSZ anode was 95 mW cm^{-2} under 5% H_2S in Ar fuel, it enhanced to 320 mW cm^{-2} under 5% H_2S in methane. This clearly indicates the synergistic behavior of H_2S containing methane fuel over doped strontium titanate catalysts.

Beck et al. [29] proposed a two step mechanism for adsorption and decomposition of H_2S over a titanium oxide surface. Based on their work, hydrogen sulfide adsorption takes place in surface oxygen vacancies. Upon adsorption, a –SH group is formed and the remaining hydrogen is donated to an adjacent oxygen or hydroxyl

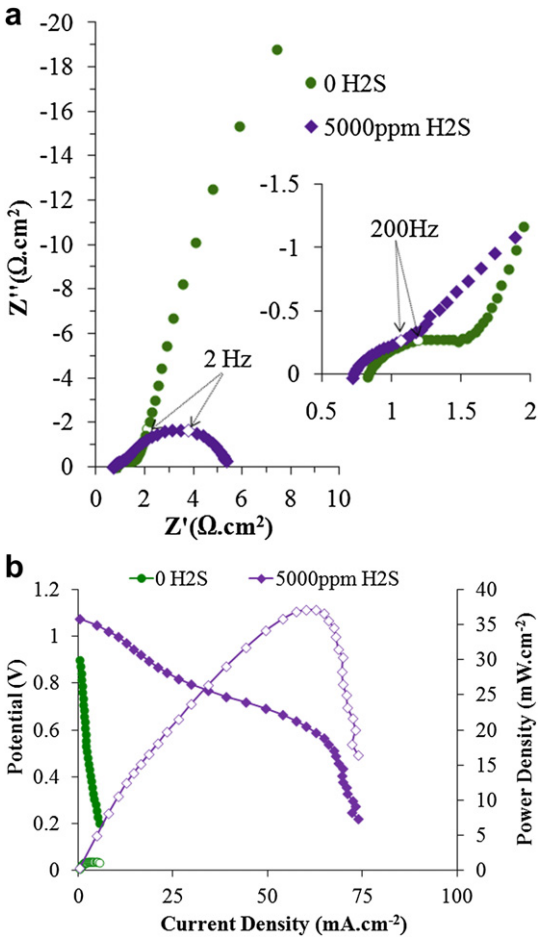

Fig. 9. Electrochemical performance of the cell with 23 wt% YST infiltrated YSZ anode: (a) open circuit impedance spectra and (b) V–i characteristics and power densities at 850 °C under humidified methane fuel with no H_2S and 0.5% H_2S.

group which eventually results in water formation. They, however, stated that as the surface oxygens are progressively consumed and the –SH groups accumulate on the surface, water formation becomes restricted. The adsorbed sulfurs can react with hydrogen and/or water to produce H_2S, with carbon to form CS_2, and with oxygen anions to form SO_2 [28]. The adsorption of sulfur plays a critical role in the activation of the catalyst [29], and could be the origin for the enhanced performance.

The electrochemical stability of a cell with a 23 wt% YST infiltrated YSZ anode under 0.7 V constant potential is illustrated in Fig. 10, for a course of 240 h at 850 °C. The potentiostatic test was originally performed under humidified hydrogen; in the 187th h of this experiment, however, the bubbler was bypassed and the test continued under dry hydrogen. A relatively sharp decrease in current density was observed during the first 2 h. Before the stability test, the YST nano particles were treated in-situ under a hydrogen atmosphere for which, the concentration of oxygen ion vacancies and Ti^{3+} is expected to be greater. Upon polarization, the concentration of these species gradually reaches a balanced state and a reasonably stable electrochemical performance is observed. A constant improvement, however, was observed in the second half of this experiment. To cast light on this, ac impedance spectra before and after the stability test were compared (not shown) and a 30% decrease was observed in charge transfer polarizarion (R1). This suggests that at the operating temperature the interface between YST and YSZ is improved which facilitates electron–ion

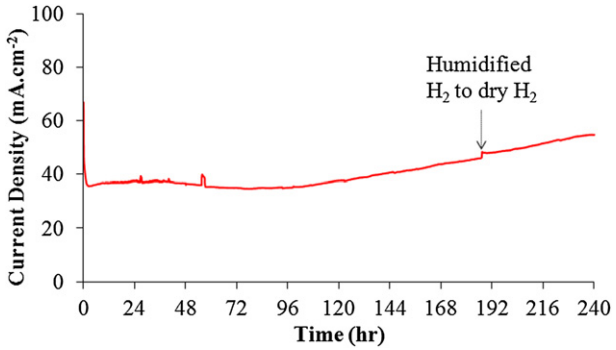

Fig. 10. Performance of the cell with 23 wt% YST infiltrated YSZ anode toward humidified and dry hydrogen under a constant voltage of 0.7 V at 850 °C for 240 h.

transfer processes occurring at the interfaces. When the humidified hydrogen was replaced by dry fuel, a sudden jump in the current density was observed and a similar improvement with time continues with the dry fuel.

Fig. 11 shows the final performance of this cell under dry hydrogen after the stability test. Several observations should be noted from this figure. First, the open circuit voltage values under dry hydrogen decrease slightly with increasing temperature. They are also remarkably higher than under humidified fuel. For example, the OCV values were 1.30 and 1.29 V with dry hydrogen, and 1.09 and 1.08 V with humidified hydrogen, respectively, at 800 and 900 °C. Second, activation polarization significantly improves with increasing temperature. If the slope of the low current density region is compared, increasing the temperature form 800–900 °C decreases the slope by a factor of 1/3. Third, the ohmic polarization also significantly decreases with temperature. This is expected because the cell is supported by a 0.3 mm YSZ electrolyte and the ionic conductivity of such a thick layer highly improves with increasing temperature. Finally, considering the facts that the cell is electrolyte supported, the relatively high ohmic resistance is not compensated, and no active electrocatalyst is incorporated, the maximum power densities are respectable.

3.4. Infiltrated YST-based anodes

As discussed earlier, it has been established that preparation and processing procedures for YST-based anodes including chemical composition, sintering temperature and sintering atmosphere critically affect cell performance [16]. On the one hand, a high temperature post-reduction process is essential to obtain a higher level of electrical conductivity; such high temperature treatment, on the other hand, leads to Ti diffusion from YST to YSZ [18]. This diffusion introduces electronic conductivity into the YSZ electrolyte which is unacceptable. It also causes a noticeable decrease in the conductivity of YST. Thus one of the main driving forces for the current research was to eliminate a high temperature sintering step by utilizing an infiltration technique. In addition, a nano-sized network of connected YST particles with remarkably larger surface area is expected to show a higher catalytic activity.

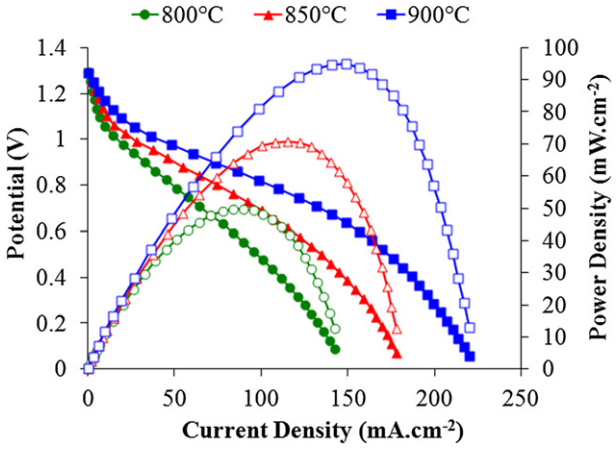

Fig. 11. *V–i* characteristics and power densities of the cell with 23 wt% YST infiltrated YSZ anode under dry hydrogen.

As this work suggests, infiltration can actually eliminate high temperature sintering and, consequently, the complications it poses. Also, it was shown here that the purity and, more importantly, the crystal size of the YST is highly dependent on the heat treatment procedure. An in-situ treatment under reducing atmosphere results in developing a pure YST phase with a crystal size as small as 16 nm. This is expected to affect the electrochemical performance of the YST-based cells as well. Kurokawa et al. [20] specified that, while YST-based materials show high electronic conductivity, they are not catalytically active to any reasonable extent. They argued that incorporation of active electrocatalysts is unavoidable with these anodes. Huang et al. [30] reported that, for an electrolyte supported cell with a YST-YSZ anode under dry fuel, the maximum power density at 900 °C was about 22 mW cm^{-2}. Also, He et al. [31] demonstrated that, for an anode-supported cell based on YST-YSZ (50:50 wt %), the maximum power density at 800 °C under dry hydrogen was only 12 mW cm^{-2}. Here, however, the maximum power density under dry hydrogen was 95 mW cm^{-2}. This is certainly not a high power density relative to conventional SOFCs; but it is much greater than the reported values for comparable cells. The clear implication of these results is that developing a nano-sized YST network over a porous YSZ scaffold with a low temperature process can bring about a respectable balance of conductivity and catalytic activity in the anode electrode which is reasonably stable as well.

4. Conclusions

The following conclusions can be drawn from the current study:

1. Using the same nominal starting composition, treatment in different temperatures and atmospheres affects not only the purity, but the crystal size of the final YST phase.
2. There is an optimum amount of infiltrated YST phase, below which the conductivity is insufficient and above which the total polarization is excessively high.
3. An infiltration technique can be successfully used to develop single phase nano-sized yttrium-doped $SrTiO_3$ within the anode electrode.
4. Under hydrogen fuel, the infiltrated cell performed with a reasonable conductivity and respectable power density in comparison with similar cells from the literature.
5. H_2S greatly improves the electrochemical performance of the fuel electrode. Under humidified methane, the performance was promoted by a factor of 35!

Acknowledgment

This work was financially supported by the Natural Sciences and Engineering Research Council of Canada (NSERC). The authors would also like to acknowledge Dr. Yadollah Maham for his valuable comments on the thermal analysis.

References

[1] A. Atkinson, S. Barnett, R.J. Gorte, J.T.S. Irvine, A.J. McEvoy, M. Mogensen, S.C. Singhal, J.M. Vohs, Nat. Mater. 3 (2004) 17.
[2] J.B. Goodenough, Y.H. Huang, J. Power Sources 173 (2007) 1.
[3] C. Sun, U. Stimming, J. Power Sources 171 (2007) 247.
[4] S.P. Jiang, S.H. Chan, J. Mater. Sci. 39 (2004) 4405.
[5] D. Simwonis, F. Tietz, D. Stover, Solid State Ionics 132 (2000) 241.
[6] Q.X. Fu, F. Tietz, Fuel Cells 8 (2008) 283.
[7] S.C. Singhal, K. Kendall, High Temperature Solid Oxide Fuel Cells: Fundamentals, Design and Application, Elsevier, Amsterdam, 2003.
[8] K. Sasaki, K. Susuki, A. Iyoshi, M. Uchimura, N. Imamura, H. Kusaba, Y. Teraoka, H. Fuchino, K. Tsujimoto, Y. Uchida, N. Jingod, J. Electrochem. Soc. 153 (2006) A2023.
[9] M.L. Toebes, J.H. Bitter, A.J. van Dillen, K.P. de Jong, Catal. Today 76 (2002) 33.
[10] C.M. Finnerty, N.J. Coe, R.H. Cunningham, R.M. Ormerod, Catal. Today 46 (1998) 137.
[11] M.D. Gross, J.M. Vohs, R.J. Gorte, J. Mater. Chem. 17 (2007) 3071.
[12] M. Gong, X. Liu, J. Trembly, C. Johnson, J. Power Sources 168 (2007) 289.
[13] J.W. Fergus, Solid State Ionics 177 (2006) 1529.
[14] A.J. Jacobson, Chem. Mater. 22 (2010) 660.
[15] S. Hui, A. Petric, J. Electrochem. Soc. 149 (2002) J1.
[16] Q. Ma, F. Tietz, D. Stover, Solid State Ionics 192 (2011) 535.
[17] Q.X. Fu, S.B. Mi, E. Wessel, F. Tietz, J. Eur, Ceram. Soc. 28 (2008) 811.
[18] Q. Ma, F. Tietz, D. Sebold, D. Stover, J. Power Sources 195 (2010) 1920.
[19] A.R. Torabi, T.H. Hanifi, P. Etsell, J. Sarkar, Electrochem. Soc. 159 (2011) B201.
[20] H. Kurokawa, L. Yang, C.P. Jacobson, L.C. De Jonghe, S.J. Visco, J. Power Sources 164 (2007) 510.
[21] M.P. Pechini, U.S. Patent No. 3,330,697 (1967).
[22] X. Lu, T.S. Pine, D.R. Mumm, J. Brouwer, Solid State Ionics 178 (2007) 1195.
[23] S.B. Adler, Solid State Ionics 111 (1998) 125.
[24] T.L. Reitz, H. Xiao, J. Power Sources 161 (2006) 437.
[25] Q.A. Huang, R. Hui, B. Wang, J. Zhang, Electrochim. Acta 52 (2007) 8144.
[26] S. Park, R. Craciun, J.M. Vohs, R.J. Gorte, J. Electrochem. Soc. 146 (1999) 3603.
[27] A. Vincent, J.L. Luo, K.T. Chuang, A.R. Sanger, J. Power Sources 195 (2010) 769.
[28] A. Vincent, J.L. Luo, K.T. Chuang, A.R. Sanger, Appl. Catal. B 106 (2011) 114.
[29] D.D. Beck, J.M. White, C.T. Ratcliffe, J. Phys. Chem. 90 (1986) 3123.
[30] X. Huang, H. Zhao, W. Qiu, W. Wu, X. Li, Energy Convers. Manage. 48 (2007) 1678.
[31] H. He, Y. Huang, J.M. Vohs, R.J. Gorte, Solid State Ionics 175 (2004) 171.